JOURNAL OF SPACECRAFT AND ROCKETS
Vol. 29, No. 5, September-October 1992

# Testing and Numerical Modeling of Hypervelocity Impact Damaged Space Station Multilayer Insulation

William Keith Rule*
*University of Alabama, Tuscaloosa, Alabama 35487*

**On orbit, Space Station Freedom will be subjected to hypervelocity impacts from space debris. These impacts will damage the multilayer insulation in addition to other components. The purpose of this investigation was to develop a simple numerical model that could be used in an engineering design environment for quickly assessing the thermal effects of hypervelocity impact damage to multilayer insulation. Thermal vacuum tests using multilayer insulation with simulated impact damage were conducted to validate the numerical model. The characteristics of the numerical model and the test results are described in this paper. The numerical model was found to adequately agree with the experimental results.**

## Nomenclature

$A_{ij}$ = area used in $F_r$ calculation, m$^2$
$a$ = perpendicular distance between surfaces for view factor calculation, m
$b$ = radius for circular radiating area for view factor calculation, m
$C_{ij}$ = thermal equilibrium coefficients, W/m$^2$K
$c$ = radius of circular absorbing area for view factor calculation, m
$D$ = diameter of the projectile, m
$D_s$ = bumper standoff distance, m
$F_{A1\text{-}A2}$ = view factor for radiating from circular area $A1$ to circular area $A2$
$F_r$ = view factor for radiating from ring area to ring area
$G$ = $b/a$
$H$ = $c/a$
$h_N$ = effective heat transfer coefficient of the Dacron netting, W/mK
$k$ = the in-plane thermal conductivity of a layer, W/mK
$q_i$ = net heat flux into the $i$th node of a layer from adjacent layers, W/m$^2$
$q_{in}$ = heat flux into a node from adjacent layers, W/m$^2$
$q_N$ = heat flux through a layer of Dacron netting, W/m$^2$
$q_{out}$ = heat flux out of a node to adjacent layers, W/m$^2$
$q_r$ = radiation heat flux, W/m$^2$
$R^2$ = coefficient of determination
$r$ = radial position of a node, m
$T$ = temperature in a layer, K
$T_b$ = bumper thickness, m
$T_{i,j}$ = temperature of the $i$th node of the $j$th layer, K
$t$ = thickness of a layer, m
$V$ = impact velocity, km/s
$\Delta$ = radial distance between nodes, m
$\epsilon$ = emissivity of a radiating surface
$\theta$ = impact angle, deg
$\sigma$ = Stefan-Boltzmann constant, W/mK

## Introduction

THIS paper describes an experimental and numerical investigation of the degradation of the insulating capabilities of the multilayer insulation (MLI) of Space Station Freedom (SSF) due to hypervelocity impact damage. The main goal of the project described here was to develop and experimentally validate a simple design tool for approximately predicting the effects of debris impact damage to SSF MLI.

A significant quantity of orbital debris has been created from abandoned spacecraft over the last three decades.[1] The size of the debris varies from virtually intact upper stages of rockets to small particles produced by explosions and impacts on orbit. Particle sizes ranging from 0.5 mm to 2 cm are potentially the most hazardous for spacecraft in low Earth orbit because these particles have a high energy content, are quite numerous, and are too small to track by radar or other means. Because these particles are traveling at hypervelocities (10–20 km/s), they can inflict severe impact damage to spacecraft. Spacecraft with long duration missions like SSF have a relatively high probability of colliding with debris particles of significant size and energy.[2]

SSF will use a Whipple[3] bumper for protection against space debris impact. This will involve placing a thin aluminum shell (the bumper) a small distance from the pressure wall. The bumper protects by breaking up or vaporizing a debris particle such that the pressure wall is impacted by a relatively benign cloud of tiny particles instead of a single lethal particle. The SSF bumper is being designed to minimize damage to the pressure wall for the most probable range of debris particle sizes and velocities.

The passive thermal control system (PTCS) of SSF consists of MLI. As the name implies, this type of insulation primarily consists of many layers of double aluminized Mylar. On SSF, the MLI will be placed between the bumper and the pressure wall. Experiments have shown that the debris cloud generated by the bumper as a result of a hypervelocity impact can produce a significant hole in the MLI blanket.

Specimens of MLI were subjected to simulated space debris impact damage in the light gas gun of the Space Debris Simulation Facility of NASA Marshall Space Flight Center (MSFC). These damaged MLI specimens were then placed in a thermal test fixture developed by the Boeing Company and tested in the simulated space environment (liquid nitrogen temperatures, $<$1.3E-3 Pa vacuum) of the Sunspot 1 Thermal Vacuum Chamber (STVC) of MSFC to determine the effects of the impact damage under steady-state thermal conditions. A numerical model was developed to simulate the behavior of the damaged MLI during thermal vacuum testing. The numerical model was calibrated with the experimental results.

There appears to be no reference to thermal vacuum testing or numerical modeling of hypervelocity impact damaged MLI in the open technical literature. Recently, undamaged MLI has been tested and modeled,[4–6] and some MLI research was per-

Received Nov. 1, 1991; revision received Feb. 20, 1992; accepted for publication Feb. 24, 1992. 

*Assistant Professor, Department of Engineering Mechanics. Member AIAA.

formed during the Apollo era.[7] Auburn University recently completed some testing for MSFC that involved manually cutting a small hole (1.27 cm) in an MLI blanket to simulate the effect of a micrometeoroid strike on a spacecraft without a bumper.[8] However, the primary focus of the Auburn study was on the thermal characteristics of MLI covered protrusions through the main MLI blanket.

## Testing Facilities at Marshall Space Flight Center

The Space Debris Simulation Facility of MSFC has been conducting impact tests for the SSF program since July 1985. This facility has a two-stage light gas gun that can launch 2.5–12.7-mm projectiles at speeds of 2–8 km/s.[9] Some of the impact test results that have been produced by this facility have recently been compiled.[10] A typical test setup is shown in Fig. 1. For this project, the MLI blanket was placed next to the bumper. Thermal testing was conducted in the STVC of MSFC. During this study, the pressure in the chamber was reduced to $<1.3E\text{-}3$ Pa and the $LN_2$ shrouds were maintained at approximately 120 K.

The Boeing Company in Huntsville, Alabama, is currently charged with designing and testing the PTCS of SSF. As part of this effort, Boeing fabricated a thermal vacuum test fixture similar in construction to a portion of the Space Station wall. Recently, an undamaged MLI blanket was tested using this fixture in the STVC.[4] This test fixture will now be described. A 4.06-$m^2$ portion of the wall structure was considered. The pressure wall was modeled using two 3.18-mm-thick 2219 AL plates welded to the edges of the bottom flange of a 6061 AL I-beam meant to represent a ring frame, Fig. 2. The curvature of SSF was not modeled and need not be for PTCS validation. Four 304 stainless steel members modeling the stringers of SSF were attached to the top flange of the ring frame. The stringers

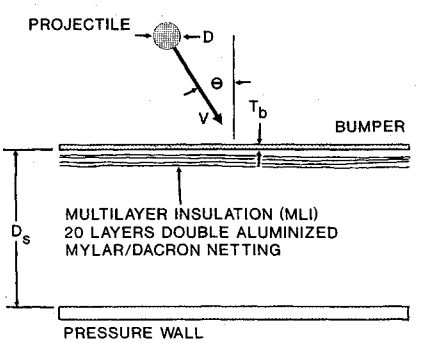


**Fig. 1 Schematic drawing of impact specimen configuration.**

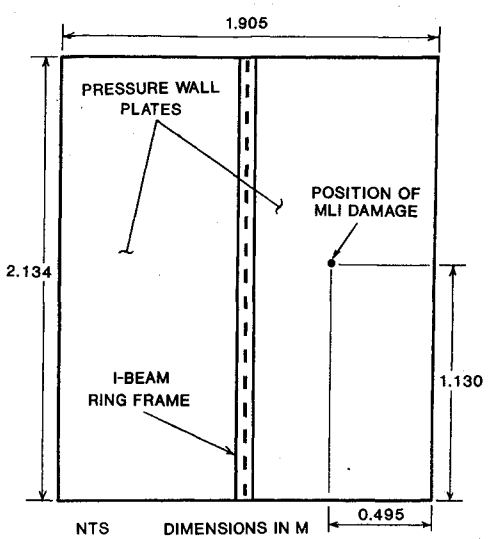


**Fig. 2 Drawing of pressure wall plate showing position of MLI damage.**

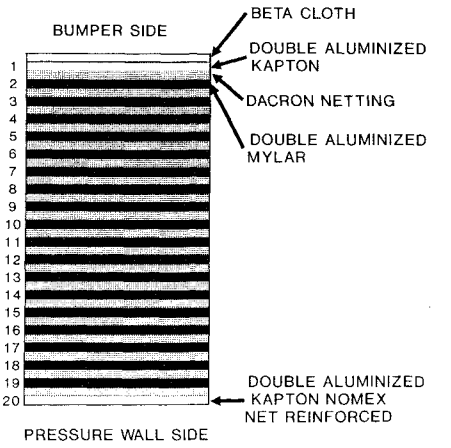


**Fig. 3 MLI lay-up used in the test fixture.**

and the ring frame provided support for the MLI blanket and the plates representing the bumper. The ends of the stringers that were not connected to the ring frame were supported on Teflon blocks. T-type (copper/constantan) thermocouples were used as temperature sensors.[11] A uniform array of strip heaters was attached to the bottom of the pressure wall structure to simulate convective heat transfer from the interior of an SSF module.

The six regions sectioned off by the ring frame and stringers were covered by six overlapping MLI blankets of identical composition. The MLI consisted of a protective outer cover of beta cloth (Teflon impregnated porous fiberglass cloth), two layers of double aluminized Kapton, and 18 layers of double aluminized Mylar, Fig. 3. Dacron netting was placed between the aluminized layers to inhibit interlayer heat transfer by conduction. Thus, radiation is the primary form of heat transfer through the MLI in the vacuum of space. Approximately 3% of the surface area of the aluminized layers was uniformly perforated to allow for degassing during launch. The model for the bumper consisted of six 1.52-mm-thick 6061 T6 aluminum sheets placed on top of the MLI. Where supported, the bumper standoff from the pressure wall was 10.2 cm. Because of the force of gravity, both the MLI blankets and the bumper plates sagged somewhat between supports.

The modeled portion of the SSF wall was placed in a shallow box supported on four legs. The depth of the box was approximately equal to the thickness of the modeled SSF wall. Heaters and thermocouples were applied to the box and supporting legs. The temperature of the box was adjusted to approximately equal that of the pressure wall plate so that the box would behave like an insulated boundary. Thus, essentially all heat applied to the pressure wall by the strip heaters was forced to radiate through the MLI and bumper to the $LN_2$ shrouds. The box was covered with a layer of MLI to further retard heat transfer between the box and the pressure wall plate. A schematic drawing of a cross section through the test fixture is shown in Fig. 4.

## Hypervelocity Impact Damaged Test Specimens

Fourteen specimens were tested in STVC. Two undamaged specimens were tested to provide a datum against which to compare the results of the damaged specimens. Table 1 summarizes the impact parameters associated with the 12 impact damaged specimens tested. Table 1 also provides some measurements of the impact damage in terms of hole diameters for the aluminized layers of the MLI and the beta cloth. These values are approximate because the holes were somewhat irregular in shape and thus difficult to measure. Most of the aluminized layers of a given specimen had approximately the same hole diameter. The beta cloth holes were typically smaller. To simplify the calculations, and because the aluminized layers provided the bulk of the insulating capabilities,

**Table 1 Impact parameters associated with the impact damaged multilayer insulation specimens**

| Data point number[a] | MSFC test number | Al 1100 projectile diameter, mm | Hall projectile velocity, km/s | Impact angle, $\theta$, deg | Al 6061-T6 bumper thickness, mm | Aluminized layers of MLI hole diameter, cm | Beta cloth hole diameter, cm |
|---|---|---|---|---|---|---|---|
| 3 | 1016 | 4.75 | 6.13 | 45 | 2.03 | 3.81 | 1.52 |
| 4 | 1028 | 6.35 | 6.98 | 0 | 1.60 | 4.83 | 3.05 |
| 5 | 1018 | 6.35 | 6.28 | 45 | 2.03 | 4.83 | 3.81 |
| 6 | 1020 | 6.35 | 6.91 | 45 | 2.03 | 4.83 | 3.05 |
| 7 | 1019 | 6.35 | 6.84 | 45 | 2.03 | 4.83 | 3.05 |
| 8 | 1027 | 6.35 | 7.05 | 0 | 1.60 | 4.83 | 2.54 |
| 9 | 1034 | 6.35 | 5.20 | 45 | 1.60 | 4.83 | 3.81 |
| 10 | 1029 | 6.35 | 4.98 | 0 | 2.03 | 5.08 | 1.52 |
| 11 | 1026 | 6.35 | 5.22 | 0 | 1.60 | 5.08 | 3.56 |
| 12 | 1035 | 6.35 | 6.21 | 45 | 1.60 | 5.08 | 3.56 |
| 13 | 1017 | 6.35 | 6.20 | 45 | 2.03 | 5.33 | 3.05 |
| 14 | 1012 | 7.95 | 6.72 | 0 | 2.03 | 5.59 | 4.06 |

[a]Data points 1 and 2 were undamaged multilayer insulation specimens.

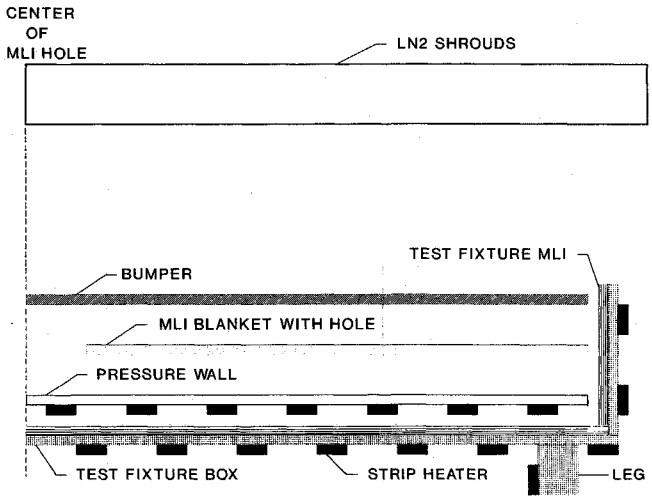


**Fig. 4 Schematic drawing of a cross section through the thermal test fixture.**

it was assumed for modeling purposes that the beta cloth hole was identical to that of the aluminized layers. Some correction of the beta cloth hole diameter was provided for with the diameter ratio parameter, as will be discussed. The impact specimens of Table 1 were not generated especially for this project. Rather, they were obtained from a program to qualify the bumper of SSF against orbital debris impacts.[10]

A typical MLI impact specimen consisted of a 30.5-cm square blanket with the impact damage in the form of a ragged, approximately circular, centrally located hole. The many layers of the MLI blanket were kept from separating during testing with a few wire staples. The impact specimens were covered with a layer of soot from the explosive charge of the light gas gun. As much of the soot as possible was removed by placing each specimen between stainless steel wire screens and carefully cleaning the specimen with a soft brush using Freon as a solvent. A sharpened section of pipe was used to cut a 30.5-cm-diam disk from each specimen. A disk shape was used in the thermal testing to preserve axial symmetry. As large a disk as possible was cut from the impact specimens to minimize the disturbing effects of the disk boundary on the heat transfer characteristics of the hole in the MLI. The 30.5-cm-diam undamaged MLI specimens were fabricated in the same fashion.

For thermal testing purposes, each 30.5-cm-diam MLI specimen was centered over a 25.4-cm-diam hole in the MLI blanket of the thermal test fixture. Thus, there was a 2.54-cm lap joint all around the outer edge of the specimen. Teflon tape was used to tape down the outer edge of the top layer (beta cloth) of the specimen to the beta cloth layer of the test fixture MLI blanket. Care was taken to tape each specimen in an identical fashion to enhance the consistency of the experimental results. Ideally, it would have been best not to have a lap joint in the MLI blanket. This was not possible due to the cost of impact testing large MLI blankets. However, some of the perturbing effects of the lap joint were filtered out of the results since the undamaged MLI disks, which provided a no-damage datum, also had a lap joint. To simplify the calculations, the presence of the lap joint was not numerically modeled in this investigation.

Unfortunately, all impact specimens available at the start of this project consisted of 30 aluminized layers (the old SSF baseline), whereas the Boeing test fixture blanket (and the new SSF baseline) consisted of a 20-layer MLI. Ideally, the MLI lay-up of the impact specimens should have been identical to that of the test fixture. However, the constituents of both blankets were identical and their insulating behavior similar. Numerical simulations of 20- and 30-layer MLI blankets with no MLI hole and typical thermal system parameters were run, and it was found that the absolute temperature of the pressure wall covered with the 30-layer blanket was only 11% higher than that of the 20-layer blanket case. To simplify the calculations, and because 98% of the test fixture was covered with a 20-layer MLI, all MLI were assumed to be a 20-layer MLI.

## Experimental Results

The testing was conducted in the following manner. Each specimen was carefully taped in place on the MLI blanket of the test fixture. The STVC was closed, evacuated to less than 1.3E-3 Pa, and the $LN_2$ shrouds were cooled to approximately 120 K. Then, 23.05 W were applied to the pressure wall, and the guard heaters on the remainder of the test fixture were energized to maintain approximately adiabatic conditions (zero temperature difference) between the pressure wall plate and the surrounding, supporting test fixture. The guard heater outputs were adjusted periodically during the testing to follow changes in the pressure wall temperatures. After allowing a brief time for stabilization, the thermocouple temperature data for the pressure wall and the bumper was collected approximately every 5 min for about 6 h. The same procedure was followed for all 14 specimens tested.

Approximately 6 h was allowed for the test fixture to come to steady-state conditions. This amount of time appeared to be adequate for most of the specimens. In any case, temperature fluctuations in the large STVC shrouds due to changes in the local environment would prohibit the attainment of perfect steady-state conditions no matter how long the experiment was allowed to run. The relatively high thermal conductivity of the pressure wall and the bumper prevented the development of large temperature gradients in these components. Thus, local temperature gradients in the vicinity of the impact damage were not large enough to characterize the degradation of the insulating capabilities of the MLI. Accordingly, only the temperatures of the thermocouples centered on the MLI impact damage were used to calibrate the numerical model.

## Numerical Model to Simulate the Behavior of Damaged Multilayer Insulation in the Thermal Vacuum Chamber

The main goal of this project was to develop a design tool to approximately predict the thermal effects of space debris impact damage to the MLI of SSF. To be suitable as a design tool requires that the program be easy to use and that the solution times be minimized to rapidly provide feedback for design and maintenance studies. These requirements dictated that the numerical model be made as simple as possible while still retaining the capability to provide physically reasonable results. The analysis technique described and validated herein has been incorporated into a user-friendly computer program. This program is suitable for on-orbit, spacecraft design studies involving changing such system parameters as the MLI hole diameter and the level of thermal radiation from space.[12]

The numerical model was based on the assumption of axial symmetry about the center of the MLI damage. A finite difference analysis scheme was used to discretize the system, where an axially symmetric ring of material can be modeled by a single node. Thus, only a single, radial line of nodes was required for each layer in the thermal system. Higher levels of accuracy can be obtained by using more nodes and spacing them closer together. The numerical model uses the same number of nodes in each layer. The time required to complete a set of calculations increases greatly as more nodes are used. The presence of the ring frames and stringers was not modeled. These would be difficult and computationally expensive to model since they would be arbitrarily placed, which would destroy the radial symmetry. Accurate studies of the effects of the ring frames and stringers would require a very detailed special purpose thermal model. Such studies are beyond the scope of the design tool under development in this study. However, the presence of the ring frame and stringers was accounted for indirectly during the thermal model calibration process, as will be discussed in the next section.

As was discussed, it was assumed that all of the MLI consisted of the same number of layers, and that no lap joints were present in the MLI. It was also assumed that the damage to the MLI consisted of a circular hole of the same diameter through all of the MLI layers. Deviations from this assumed ideal hole geometry are provided by an experimentally determined parameter called the diameter ratio, which is described in the next section. Each layer of the MLI was explicitly modeled with an array of nodes except for the beta cloth and outer Kapton layers. These layers were modeled as a single layer since there was no Dacron netting layer to separate them. Thus, for the insulation system tested, 22 layers had to be modeled: the pressure wall, 19 aluminized MLI layers, the combined Kapton-beta cloth layer, and the bumper layer. The STVC was modeled as a single node with one set of effective properties.

The numerical model was designed to treat steady-state conditions. This means that the heat flux into each node must equal the heat flux out of that node. Thus, an equation can be written for each node to calculate the nodal temperature such that the heat influx will equal the heat outflow. In a vacuum, the modes of heat transfer are conduction and radiation. Since radiation heat transfer is a function of temperature to the fourth power, the nodal heat flux equilibrium equations are nonlinear and must be solved by an iterative process. The thermal equilibrium equations are coupled as well—the temperature of a given node depends on the temperature of adjacent nodes in the same layer as well as the nodal temperatures of adjacent layers.

The following equation[13] can be written to describe thermal equilibrium at a node:

$$-\frac{kt}{r}\frac{dT}{dr} - kt\frac{d^2T}{dr^2} = q_{in} - q_{out} = q_i \tag{1}$$

This equation states that the heat conducted away from a node in the plane of the layer must equal the net influx of heat to that node from adjacent layers. The temperature derivatives were represented by finite difference approximations using the temperatures of three adjacent nodes in a layer in the usual fashion:

$$\frac{dT}{dr} = \frac{T_{i+1} - T_{i-1}}{2\Delta} \tag{2}$$

$$\frac{d^2T}{dr^2} = \frac{T_{i+1} - 2T_i + T_{i-1}}{\Delta^2} \tag{3}$$

For the case of a layer with no hole, axial symmetry dictates that the in-plane heat flux through the origin must be zero. Also, layers with a hole have no in-plane heat flux at the free edge. Considering the form of Eqs. (2) and (3), these boundary conditions can be satisfied by setting the temperatures of the first two nodes of a layer equal to that of the third node. Similarly, there was no in-plane heat flux at the outer free edge of the modeled area. Here, the temperatures of the outer two nodes were set equal to that of the third node from the outer free edge.

Substituting Eqs. (2) and (3) into Eq. (1) produces the following equation, which describes thermal equilibrium at the $i$th node of a layer:

$$T_{i-1}\left(\frac{kt}{2r_i\Delta} - \frac{kt}{\Delta^2}\right) + T_i\left(\frac{2kt}{\Delta^2}\right) + \left(-\frac{kt}{2r_i\Delta} - \frac{kt}{\Delta^2}\right) = q_i \tag{4}$$

Equation (4) can be written in a more compact form as

$$C_{i1}T_{i-1} + C_{i2}T_i + C_{i3}T_{i+1} = q_i \tag{5}$$

where the $C_{ij}$ are thermal equilibrium coefficients that can be determined from Eq. (4). Equation (5) can be expanded in matrix fashion to represent an entire layer of nodal temperatures:

$$\begin{bmatrix} C_{22} & C_{23} & 0 & 0 & 0 & 0 & 0 \\ C_{31} & C_{32} & C_{33} & 0 & 0 & 0 & 0 \\ 0 & C_{41} & C_{42} & C_{43} & 0 & 0 & 0 \\ \vdots & \vdots & \vdots & \vdots & \vdots & \vdots & \vdots \\ 0 & 0 & 0 & 0 & C_{(N-2)1} & C_{(N-2)2} & C_{(N-2)3} \\ 0 & 0 & 0 & 0 & 0 & C_{(N-1)1} & C_{(N-1)2} \end{bmatrix} \begin{Bmatrix} T_2 \\ T_3 \\ T_4 \\ \vdots \\ T_{N-2} \\ T_{N-1} \end{Bmatrix} = \begin{bmatrix} q_2 - C_{12}T_1 \\ q_3 \\ q_4 \\ \vdots \\ q_{N-2} \\ q_{N-1} - C_{(N-1)3}T_N \end{bmatrix} \tag{6}$$

Equation (6) consists of a tridiagonal system of equations that can be solved very efficiently. Note that $T_1$ (at the edge of the MLI hole) and $T_N$ (at the outer edge of the modeled area) are not explicitly solved for, rather they are set equal to $T_3$ and $T_{N-2}$, respectively, of the previous iteration, as was mentioned in the boundary condition discussion. An iterative procedure was required to solve Eq. (6) because the $q_i$ values are complicated nonlinear functions of the nodal temperatures.

The solution procedure consisted of solving Eq. (6) for the nodal temperatures of the first layer (pressure wall) and then proceeding to the next layer, solving for the nodal temperatures, and so forth, until finally solving for the nodal temperatures of the final layer (bumper). This procedure was re-

peated until the nodal temperatures converged within a small tolerance. The calculation of the $q_i$ values will now be discussed. The formulas used to calculate the $q_i$ values varied from layer to layer.

**Pressure Wall Heat Flux Calculations**

Every node of the pressure wall was assumed to receive the same magnitude of heat flux from the pressure wall strip heaters since they were uniformly distributed over the bottom surface of the pressure wall. The magnitude of this heat influx was determined by dividing the total strip heater input to the pressure wall by the total area of the pressure wall.

The pressure wall radiated heat toward the MLI blanket. This heat flux is described by the following equation[13]:

$$q_r = \epsilon\sigma T_i^4 \tag{7}$$

Emissivity values can vary between 0 and 1 depending on the material the surface is made from and the condition of the surface (polished or tarnished, and so forth). Emissivities can vary as a function of time and temperature. In this investigation, all emissivities were assumed to be constant. The pressure wall was exposed to heat flux radiated from the adjacent MLI layer and from the bumper if an MLI hole is present. Only a portion of the radiation impinging on the pressure wall was absorbed. The fraction absorbed is called the absorptivity, and it is commonly assumed to equal the emissivity.[13] Radiated energy that is not absorbed is reflected. The computer model was designed to track the magnitudes of all emitted, absorbed, and reflected radiation to preserve conservation of energy.

First, consider the simplest case of no MLI hole. Here, all of the nodal temperatures of the MLI layer next to the pressure wall will be identical after equilibrium is attained. Thus, the thermal radiation emitted and reflected will be the same for each node in the MLI layer. Also, no thermal energy from the bumper will strike the pressure wall. Accordingly, for this simple case, the computer program used the thermal radiation (both emitted and reflected) from the $i$th node of the MLI layer next to the pressure wall when calculating the heat influx to the $i$th node of the pressure wall.

The more general case with a hole in the MLI is considerably more complicated. Here, the thermal radiation coming from each node of the MLI layer next to the pressure wall will vary. Also, some of the thermal radiation given off by the bumper will pass through the hole in the MLI and strike the pressure wall plate. The concept of view factors[13] was used to treat this problem.

View factors give the fraction of the thermal radiation given off from a surface that will strike another surface of known geometry and orientation. Consider the case where thermal energy is radiating from a circular area $A_1$ (of radius $b$) to a circular area $A_2$ (of radius $c$), where the planes of areas are

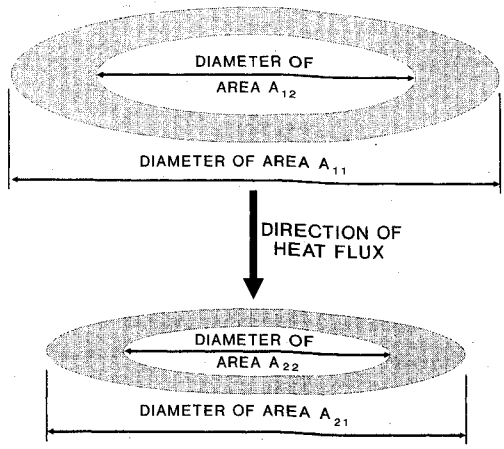


**Fig. 5 Schematic drawing of ring-to-ring view factor geometry.**

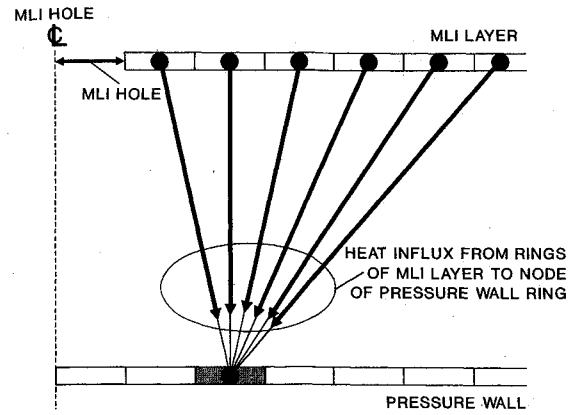


**Fig. 6 Schematic drawing illustrating the method of calculating the heat flux from rings of first MLI layer to a node in a pressure wall ring.**

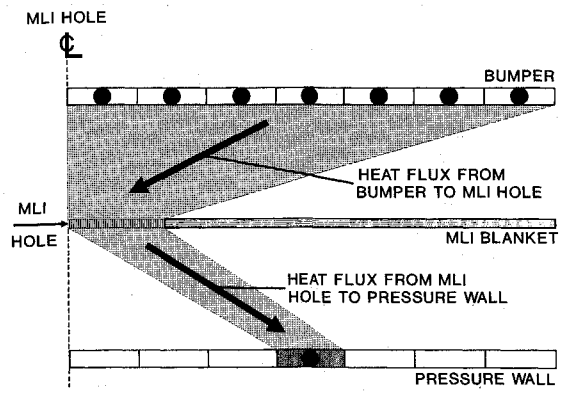


**Fig. 7 Schematic drawing illustrating the method of calculating the heat flux to the pressure wall from the bumper through the MLI hole.**

parallel, separated by a distance $a$, and the areas are centered over each other. The view factor associated with this geometry, $F_{A1-A2}$, is[13]

$$F_{A1-A2} = \frac{1 + G^2 + H^2 - [(1 + G^2 + H^2)^2 - 4G^2H^2]^{1/2}}{2G^2} \tag{8}$$

where $G = b/a$ and $H = c/a$. This investigation was based on the assumption of axial symmetry, and so a view factor $F_r$ for radiating from ring to ring is required (see Fig. 5):

$$F_r = \frac{A_{11}(F_{A11-A21} - F_{A11-A22}) - A_{12}(F_{A12-A21} - F_{A12-A22})}{A_{11} - A_{12}} \tag{9}$$

Thus, $F_r$ specifies the fraction of the energy that is radiated by $\Delta A_1$ ($= A_{11} - A_{12}$) that will strike $\Delta A_2$ ($= A_{21} - A_{22}$).

The total heat influx to the ring corresponding to the $i$th node of the pressure wall from the adjacent MLI layer was calculated by a summation formed from repeatedly using Eq. (9) for each node (and thus corresponding ring) of the MLI layer. This is illustrated schematically in Fig. 6. The heat influx from the bumper to the pressure wall was treated in two steps. First the ring approach of Eq. (9) was used to calculate the total heat influx to the MLI hole from each node on the bumper. For this calculation, $A_{22}$ (Fig. 5) was set to zero and $A_{21}$ corresponded to the area of the MLI hole. Then this total heat influx to the MLI hole was allocated to the pressure wall node under consideration by using Eq. (9) again. For this calculation, $A_{12}$ was set to zero and $A_{11}$ was set equal to the area of the MLI hole. This process is illustrated in Fig. 7.

**Heat Flux Calculations for MLI Layer Next to Pressure Wall**

The MLI layer next to the pressure wall (first MLI layer) can radiate energy to both the pressure wall and the next MLI

**Table 2 Typical results showing the sensitivity of the calculated pressure wall temperature to mesh density at the multilayer insulation damage position**

| Number of nodes per layer | Reciprocal of number of nodes per layer | Calculated pressure wall temperature, K | Interpolated pressure wall temperature, K | Percentage error with respect to extrapolated pressure wall temperature |
|---|---|---|---|---|
| 5 | 0.2000 | 306.00 | 306.07 | 0.41 |
| 9 | 0.1111 | 305.62 | 305.48 | 0.29 |
| 17 | 0.0588 | 305.13 | 305.13 | 0.13 |
| 33 | 0.0303 | 304.89 | 304.94 | 0.05 |
| 65 | 0.0154 | 304.83 | 304.85 | 0.03 |
| Infinity | 0 | — | 304.74 | 0.00 |

**Table 3 Values of parameters used in the numerical model**

| | |
|---|---|
| 0.0 | >MLI hole diameter, m |
| 5.08E-2 | >MLI standoff, m |
| 23.05 | >Total heater input to pressure wall, W |
| 4.0645 | >Total pressure wall area, m |
| 0.804 | >Radius of area modeled, m |
| 3.175E-3 | >Pressure wall thickness, m |
| 6.35E-6 | >Average aluminized layer thickness of MLI, m |
| 5.08E-5 | >Beta cloth thickness, m |
| 1.524E-3 | >Bumper thickness, m |
| 1.016E-1 | >Bumper standoff, m |
| 120 | >Effective sunspot shroud temperature, K |
| 130 | >Pressure wall thermal conductivity, W/mK |
| 50 | >MLI aluminized layer thermal conductivity, W/mK |
| 1.0687 | >Effective heat transfer coefficient of Dacron netting, W/mK |
| 5 | >Beta cloth thermal conductivity, W/mK |
| 115 | >Bumper thermal conductivity, W/mK |
| 0.06 | >Pressure wall emissivity |
| 0.06 | >MLI aluminized layer emissivity |
| 0.94 | >Beta cloth emissivity |
| 0.04 | >Bumper emissivity outward |
| 0.14 | >Bumper emissivity inward |
| 0.90 | >Effective sunspot shroud emissivity |
| 5.6697E-8 | >Stefan-Boltzmann constant, W/mK |

layer. Thus, the $q_r$ for this layer will be twice that given by Eq. (7). The pressure wall can subject the nearest MLI layer to both emitted and reflected thermal radiation. This was dealt with in the same way that MLI heat flux impinging on the pressure wall was treated (reverse of Fig. 6), which has been discussed. Note that the MLI layer next to the pressure wall is blocked from directly receiving radiation from the bumper.

The MLI layer nearest the pressure wall will also be subjected to emitted and reflected radiation from the next MLI layer (second MLI layer). Since the MLI layers are so close to each other, the view factor approach of Eq. (9) was not required here. The thermal radiation flux from the second MLI layer striking the $i$th node of the first MLI layer was assumed to equal the thermal radiation flux from the $i$th node of the second MLI layer.

Conduction between the first and second MLI layers was inhibited, but not stopped, by the presence of a layer of Dacron netting. The heat flux to the $i$th node of the first MLI layer from the $i$th node of the second MLI layer through the Dacron netting $q_N$ was assumed to be of the following form:

$$q_N = h_N(T_{i,2} - T_{i,1}) \tag{10}$$

A value for the effective netting heat transfer coefficient $h_N$ was determined by fitting the computer model to the experimental data. It was assumed that the netting heat transfer coefficient was the same for all netting layers.

#### Heat Influx Calculations for a Typical Aluminized MLI Layer

Here the net heat influx $q_i$ to the nodes of the MLI layers between the first (next to pressure wall) and last (next to bumper) MLI layers are considered. The $q_i$ values for the nodes of these layers are calculated in a similar fashion to what was done for the first MLI layer, except here there are two MLI layers radiating into the MLI layer under consideration. No view factor calculations are required since the layers are assumed to be close together. Also, there are two layers of Dacron netting next to each MLI layer, and thus, Eq. (10) will have to be applied twice—once for the layer above and once for the layer below.

#### Heat Influx Calculations for MLI Layer Next to Bumper

As was noted previously, the last aluminized MLI layer (closest to bumper) and the beta cloth layer were not separated by a layer of Dacron netting, Fig. 3. Accordingly, these layers were analyzed as a single layer with the inside surface having the emissivity of an aluminized layer and the outside surface having the emissivity of the beta cloth layer. The thermal conductivity of the layer was assumed to equal the weighted average (on the basis of thickness) of the two layers. For $q_i$ calculation purposes, this combined layer was treated in exactly the same manner as the first MLI layer except that here the bumper takes the place of the pressure wall.

#### Heat Influx Calculations for the Bumper Layer

The net heat influx to the bumper layer was calculated in a very similar manner to that of the pressure wall. The bumper was subjected to heat influx from the pressure wall through the MLI hole just as the pressure wall was from the bumper. However, unlike the pressure wall, there were no strip heaters on the bumper. Instead, the bumper interacted in a thermal radiation sense with the $LN_2$ shrouds of STVC. The shrouds were treated as a single node, and averaged properties were used.

This concludes the discussion of the $q_i$ calculation for the various layers of the thermal system.

Table 2 shows the results of a convergence study. Here 5, 9, 17, 33, and 65 nodes per layer were successively used in the calculations. The resulting pressure wall temperatures under the center of the MLI hole are reported. A 2.54-cm-diam MLI hole and typical SSF baseline thermal properties were used in the convergence study. Table 2 also shows interpolated temperatures based on a successful ($R^2 = 0.97$) linear fit through the temperature data using the reciprocal of the number of nodes per layer as the independent parameter. The fitted line was used to extrapolate the temperature (304.74 K) for the case of an infinite number of nodes per layer, the theoretically exact answer, where the independent parameter is set to zero ($1/\infty$). On the basis of this extrapolated temperature, percentage errors for the calculated temperatures were determined and are also listed in Table 2. Note that even the coarsest mesh had a relatively small error.

## Numerical Analysis of the Experimental Data

The results of analyzing the experimental data using the numerical model are discussed in this section. The purpose of this analysis is to show that the numerical model can be made to adequately represent the behavior of the thermal system and to empirically fit parameters associated with the thermal

**Table 4 Thermal test data analysis results**

| Data point | MSFC test number | MLI hole diameter, cm | Measured pressure wall temperature, K | Calculated pressure wall temperature, K | Measured bumper temperature, K | Calculated bumper temperature, K | Best fit Sunspot temperature, K | Best Fit diameter ratio |
|---|---|---|---|---|---|---|---|---|
| 1 | Undamaged | 0.00 | 303.3 | 305.9 | 133.8 | 133.0 | 118.3 | Undamaged |
| 2 | Undamaged | 0.00 | 306.3 | 306.5 | 135.1 | 135.1 | 121.1 | Undamaged |
| 3 | 1016 | 3.81 | 307.8 | 305.8 | 134.6 | 135.1 | 121.4 | 0.600 |
| 4 | 1028 | 4.83 | 303.8 | 303.8 | 133.9 | 133.9 | 120.0 | 0.746 |
| 5 | 1018 | 4.83 | 300.8 | 300.8 | 132.3 | 132.3 | 118.3 | 1.068 |
| 6 | 1020 | 4.83 | 300.9 | 300.9 | 133.2 | 133.2 | 119.6 | 1.090 |
| 7 | 1019 | 4.83 | 299.2 | 299.1 | 134.9 | 134.9 | 122.3 | 1.370 |
| 8 | 1027 | 4.83 | 300.4 | 300.4 | 133.4 | 133.3 | 119.9 | 1.160 |
| 9 | 1034 | 4.83 | 303.6 | 303.6 | 134.0 | 134.0 | 120.2 | 0.769 |
| 10 | 1029 | 5.08 | 304.8 | 304.7 | 133.9 | 133.9 | 119.8 | 0.600 |
| 11 | 1026 | 5.08 | 298.0 | 298.3 | 135.1 | 135.0 | 122.7 | 1.400 |
| 12 | 1035 | 5.08 | 303.9 | 303.9 | 133.9 | 133.8 | 119.9 | 0.693 |
| 13 | 1017 | 5.33 | 300.8 | 300.8 | 134.0 | 134.0 | 120.8 | 1.030 |
| 14 | 1012 | 5.59 | 306.2 | 304.5 | 133.9 | 134.3 | 120.4 | 0.600 |

Best fit Dacron netting heat transfer coefficient = 1.0687 W($m^2$K)

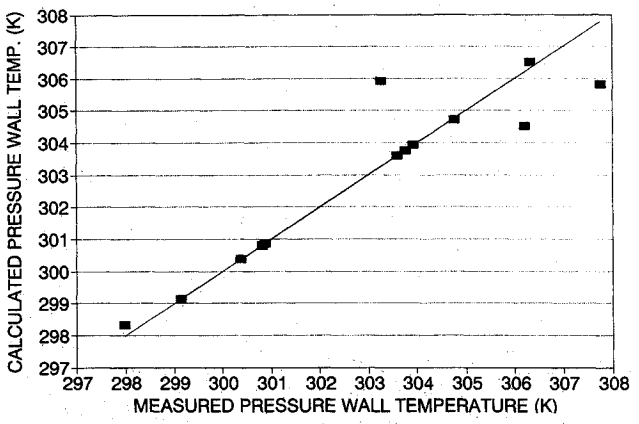


**Fig. 8 Calculated vs measured pressure wall temperatures at the MLI damage position.**

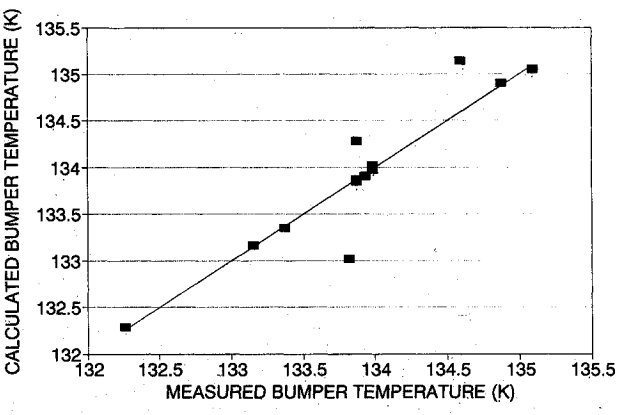


**Fig. 9 Calculated vs measured bumper temperatures at the MLI damage position.**

system. The end product of analyzing the experimental data is a validated and calibrated numerical model that can be used for making predictions of system behavior. More details on the calibration procedure that was used are provided in Ref. 14. The input parameters used by the numerical model are listed in Table 3. The values of the parameters used were typical handbook values except where noted.

The MLI hole diameter refers to the approximate diameter of the hole in the aluminized layers of the MLI. The MLI standoff is the distance between the MLI blanket and the pressure wall. For all of the testing associated with this investigation, 23.05 W were applied to a total pressure wall area of 4.065 $m^2$. The test specimen was essentially divided into two equal areas thermally due to the presence of the ring frame. Thus, only one half of the pressure wall area was modeled (2.03 $m^2$). The model developed here is based on the assumption of axial symmetry, and so the modeled area was treated as an equivalent circular region of the same size. The radius of the modeled area used in the calculations was $(2.03/\pi)^{1/2}$ = 0.804 m. The layer thicknesses used in the numerical model were based on values reported by Solomon[4] and Buitekant.[11] The bumper standoff is the distance that the bumper is separated from the pressure wall. The emissivity values used in the numerical model were all obtained from Solomon.[4] The bumper's two surfaces had different emissivities because the surface farthest from the pressure wall had a special thermal coating.

Three parameters had to be fitted from the experimental data: the diameter ratio associated with each data point, the effective Sunspot shroud temperature associated with each data point, and the effective heat transfer coefficient of the Dacron netting that was assumed to be the same for all specimens tested. The results of the thermal test data reduction are given in Table 4, and plots of calculated vs measured pressure wall and bumper temperatures are shown in Figs. 8 and 9, respectively. The plots had $R^2$ values of 0.85 and 0.88 for the pressure wall and bumper data, respectively, which indicates that the numerical model predicts the experimentally measured behavior adequately.

The diameter ratio is defined as the apparent hole diameter, as determined by running the numerical model to determine the best fit to the experimental data, divided by the measured average diameter of the hole in the aluminized layers. Thus, the diameter ratio is an empirical multiplier for the actual (physically measured) hole diameter. It is intended to account for three effects:

1) The diameter of the hole in the beta cloth is somewhat different from that of the aluminized layers. In the numerical model, it is assumed that all MLI layers have the same hole diameter.

2) The damage to the aluminized layers extended some distance back from the apparent edge of the MLI hole. This damage typically takes the form of crinkling, melting, and tearing of the delicate aluminized layers due to the intense heat and shock waves generated by the impact.

3) The MLI blanket had a finite thickness. This was not modeled numerically.

It was assumed that the diameter ratio can be correlated to the impact parameters such as particle diameter, velocity, and so forth. The idea is to use the results of this investigation to predict suitable diameter ratios for use in future design studies. The diameter ratio was allowed to vary between 0.6 and 1.4 during the parameter adjustment process. Diameter ratios beyond these bounds were not considered to be physically reasonable.

Some means of determining the appropriate diameter ratio for a given set of impact parameters is required. This was accomplished by fitting an empirical function through the diameter ratio data of Table 4:

$$\text{diameter ratio} = D[0.1978V^{3.466}T_b^{5.356}D_s(\cos\theta)^{1.694} + 2.575] \quad (11)$$

The form of Eq. (11) was discussed by Rule and Hayashida.[15] A linear plot of predicted [Eq. (11)] vs calculated (Table 4) best fit diameter ratio had an $R^2$ value of 0.48. The lack of good fit between the predicted and calculated is probably due to the scatter in the thermal data and, thus, some error in the calculated best fit diameter ratios. Also, the assumed functional form of Eq. (11) is not exact. Equation (11) should only be used to determine diameter ratios for impact conditions similar to those of this investigation. Otherwise, new numerical coefficients must be fit from an appropriate set of experimental results or a diameter ratio of unity can be used as an approximation.

Precise control of the $LN_2$ shroud temperatures was not possible for the large STVC. Thus, the shroud temperatures varied somewhat from specimen to specimen and while a given specimen was being tested. Also, it was not clear how to determine an appropriate single effective shroud temperature, which is required for the computer program, based on the measured temperatures of the six shrouds. Hence, the effective shroud temperature was considered to be an adjustable parameter in each of the 14 specimens tested. The fitted values (Table 4) varied between 118.3 and 122.7 K. Solomon[4] presented results showing that the measured STVC shroud temperatures typically vary somewhat erratically between 89 and 122 K during testing. Thus, the fitted values of the shroud temperatures seem reasonable.

The effective heat transfer coefficient of the Dacron netting (1.0687 W/m$^2$K) was determined by fitting the computed results to the experimentally measured values. For comparison, an approximate value for the netting heat transfer coefficient was developed as follows. Based on a microscopic examination of a sample of the netting, the netting was assumed to consist of a square mesh of 0.2-mm-diam fibers on 3-mm centers. The thermal conductivity of the Dacron at temperatures encountered in the Sunspot chamber was assumed to equal 0.1 W/mK.[16,17] The Dacron netting was also assumed to have uninterrupted contact with two adjacent MLI layers. Based on these assumptions, and using classical heat transfer calculation techniques, the estimated heat transfer coefficient of the Dacron netting was 67 W/m$^2$K. However, the aluminized layers of the MLI tend to crinkle somewhat, and the netting is not perfectly flat since it is woven. Thus, far less than perfect contact between the netting and the adjacent layers would be expected. Accordingly, the value of the effective heat transfer coefficient for the netting obtained from fitting the numerical model to the experimental data, 1.0687 W/m$^2$K, seems reasonable.

## Conclusions and Recommendations

During the course of this study, the following conclusions were reached.

1) The damaged MLI specimens were created (impacted) and thermally tested under as realistic conditions (with respect to SSF) as were possible.

2) The goal of realistic testing conditions prevented some of the thermal system parameters from being tightly controlled, which produced some scatter in the measured data.

3) The behavior of the thermal test fixture and specimens was adequately represented by an axially symmetric numerical model that was developed during the course of this investigation.

4) The proposed parameter, diameter ratio, provides a convenient and practical means of converting a measured MLI hole diameter to a thermally apparent MLI hole diameter.

5) The impact damaged MLI analysis technique described and validated herein has been incorporated into a computer program that is suitable for on-orbit spacecraft design studies involving changing such system parameters as the MLI hole diameter and the level of thermal radiation from space. The degradation of the insulating capabilities of the MLI of SSF due to a hypervelocity impact with space debris can be assessed by running this program with appropriate system parameters.

If more consistent data is desired, then it is recommended that a new test fixture be developed to provide a means of more tightly controlling or simplifying the thermal parameters associated with the test fixture. It is also recommended that more than 6 h be budgeted for the specimens to reach equilibrium in the vacuum chamber.

## Acknowledgments

This project was supported by NASA Contract NAS8-38555. The author wishes to thank Ben Hayashida, Scott Hill, Pedro Rodriguez, and Paul Thompson of MSFC for providing the experimental data. Joe McConnell of MSFC provided guidance with the design of the test setup. Alan Buitekant and Jeff Sharp of Boeing were very helpful during the testing phase.

## References

[1]Kessler, D. J., "Predicting Debris," *Aerospace America,* June 1988, pp. 22,23.

[2]Griffin, M. D., and French, J. R., *Space Vehicle Design,* AIAA Education Series, AIAA, Washington, DC, 1991, p. 77-81.

[3]Whipple, F. L., "Meteorites and Space Travel," *Astronomical Journal,* Vol. 52, March 1947, p. 5.

[4]Solomon, M., "Passive Thermal Control System (PTCS) Development Test Analysis Report," Boeing Co., 2-H8T4-RSB-071/90, Huntsville, AL, Nov. 1990.

[5]Bapat, S. L., Narayankhedkar, K. G., and Lukose, T. P., "Performance Prediction of Multilayer Insulation," *Cryogenics,* Vol. 30, Aug. 1990, pp. 700-710.

[6]Bapat, S. L., Narayankhedkar, K. G., and Lukose, T. P., "Experimental Investigations of Multilayer Insulation," *Cryogenics,* Vol. 30, Aug. 1990, pp. 711-719.

[7]Streed, E. R., Cunnington, G. R., and Zierman, C. A., "Performance of Multilayer Insulation Systems for the 300° to 800° K Temperature Range," *Thermophysics and Temperature Control of Spacecraft and Entry Vehicles,* Vol. 18, Progress in Astronautics and Aeronautics, AIAA, New York, 1966, pp. 735-757.

[8]Rodriguez, P. I., private communication, NASA Marshall Space Flight Center, Huntsville, AL, Feb. 1990.

[9]Taylor, R. A., "A Space Debris Simulation Facility for Spacecraft Materials Evaluation," *SAMPE Quarterly,* Vol. 18, Feb. 1987, pp. 28-34.

[10]Schonberg, W. P., Bean, A. J., and Darzi, K., "Hypervelocity Impact Physics," NASA CR-4343, Jan. 1991.

[11]Buitekant, A., "PTCS Initial Thermal/Vacuum Development Test, Phases I and II," Boeing Co., D683-10491-1, Huntsville, AL, June 1990.

[12]Rule, W. K., and Giridharan, V., "MLITEMP—A Computer Program to Predict the Thermal Effects Associated with Hypervelocity Impact Damage to Space Station MLI," NASA CR-184245, Sept. 1991.

[13]Ozisik, M. N., *Heat Transfer A Basic Approach,* McGraw-Hill, New York, 1985, pp. 1-14, 23-37, 593-642.

[14]Rule, W. K., and Hayashida, K. B., "SUNSPOT—A Program to Model the Behavior of Hypervelocity Impact Damaged Multilayer Insulation in the Sunspot Thermal Vacuum Chamber of Marshall Space Flight Center," NASA TM-103570, Jan. 1992.

[15]Rule, W. K., and Hayashida, K. B., "Empirical Predictions of Hypervelocity Impact Damage to the Space Station," NASA TM-103550, July 1991.

[16]Steere, R. C., "Thermal Properties of Thin Film Polymers by Transient Heating," *Journal of Applied Physics,* Vol. 37, No. 9, 1966, pp. 3338-3344.

[17]Assfalg, A., "Study of the Thermal Conductivity and Specific Heat of Amorphous and Partially Crystalline Poly(Ethylene Terephthalate) in Relation to Its Structure," *Journal of Physics and Chemistry of Solids,* Vol. 36, No. 12, 1975, pp. 1389-1396.

Earl A. Thornton
*Associate Editor*